Appl. Phys. B 60, 355–362 (1995)

Applied Physics B Lasers and Optics



# LIDAR multiple scattering from clouds

**L. R. Bissonnette[1], P. Bruscaglioni[2], A. Ismaelli[2], G. Zaccanti[2], A. Cohen[3,*], Y. Benayahu[4], M. Kleiman[5], S. Egert[5], C. Flesia[6], P. Schwendimann[7], A. V. Starkov[8,**], M. Noormohammadian[9], U. G. Oppel[9], D. M. Winker[10], E. P. Zege[11], I. L. Katsev[11], I. N. Polonsky[11]**

[1] DREV-Defence Research Establishment Valcartier, P.O. Box 8800, Courcelette, Québec, Canada G0A 1R0
(Fax: +1-418/844-4511; E-mail: LBISSON@sv0.drev.dnd.ca)
[2] Dipartimento di Fisica dell'Universitá, Via Santa Marta 3, I-50139 Firenze, Italy
(Fax: +39-55/483750)
[3] Department of Atmospheric Sciences, Hebrew University, Jerusalem, Israel
(Fax: +972-2/666804, E-mail: ARIEL@vms.huji.ac.il)
[4] SOREQ Nuclear Research Center, Yavne, Israel
[5] Israel Institute for Biological Research, Ness-Ziona, Israel
[6] Groupe de Physique Appliquée, Université de Genève, CH-1211 Genève 4, Switzerland
(Fax: +41-22/781-0980, E-mail: FLESIA@sc2a.unige.ch)
[7] Defence Procurement and Technology Group, System Analysis Division, CH-3000 Bern, Switzerland
[8] Computing Center, Siberian Division, Russian Academy of Sciences, Novosibirsk, Russia
[9] Mathematisches Institut der Ludwig-Maximilians Universität München, Theresienstr. 39, D-80333 München, Germany
(Fax: +49-8153/89217, E-mail: ULRICH.OPPEL@mathematik.uni-muenchen.d400.de)
[10] Atmospheric Sciences Division, NASA Langley Research Center, Mail Code 475, Hampton, VA 23665-5225, USA
(Fax: +1-804/864-2671)
[11] Institute of Physics, Pr. F. Scorina 70, 220602 Minsk, Belarus
(Fax: +7-0172/393131, E-mail: KATKOV@adonis.ias.msk.su)

Received: 3 September 1994/Accepted: 19 September 1994

**Abstract.** Multiple-scattering LIDAR return calculations obtained by seven different models for the same specified numerical experiment are compared. This work results from an international joint effort stimulated by the workshop group called MUSCLE for MUltiple SCattering Lidar Experiments. The models include approximations to the radiative-transfer theory, Monte-Carlo calculations, a stochastic model of the process of multiple scattering, and an extension of Mie theory for particles illuminated by direct and scattered light. The model solutions are similar in form but differ by up to a factor of 5 in the strength of the multiple-scattering contributions. Various reasons for the observed differences are explored and their practical significance is discussed.

**PACS:** 42.60

In many applications, light propagation in aerosol media can be described with acceptable accuracy by single-scattering methods. However, if the particles are dense enough, a sufficient number of scattered photons assumed to be lost in the single-scattering framework can reach the target or enter the receiver aperture by rescatterings. Depending on geometry and aerosol properties, this multiple-scattering effect can contribute significantly to the measured transmitted and backscattered radiation and give rise to adverse but, in some cases, potentially useful signals.

Multiple-scattering effects on LIDAR returns were demonstrated by the pioneering work of Donchenko et al. [1] and Kaul and Samokhvalov [2], and on laser transmission by Bucher and Lerner [3] and Mooradian et al. [4]. The latter two groups measured effects such as pulse delay, pulse stretching, off-axis detection and attenuation coefficient dependent on the receiver field of view. The evidence of multiple-scattering contributions in cloud LIDAR returns was also shown by Allen and Platt [5] with a center-blocked field stop to restrict the receiver field of view to a region outside of the transmitted beam, and by Pal and Carswell [6] through detection of the cross-polarized component of the LIDAR signals. Systematic measurements of multiple-scattering LIDAR returns were subsequently made by Bissonnette and Hutt [7] and Werner et al. [8]. Multiple scattering was also observed to cause spatial frequency fading of images [9, 10], and reduction of the apparent extinction in snowfalls [11–13].

Atmospheric measurements are often flawed by a poor knowledge of and control on the governing parameters. As a result, the early atmospheric experiments were soon followed by a multiplicity of laboratory simulations to separate the various effects and study their dependence on the particle properties and application geometry. For example, the multiple-scattering contributions to transmission and backscatter were extensively studied in laboratory-generated water droplet clouds

* *Present address:* Department of Physics and Atmospheric Sciences, Drexel University, Philadelphia, PA 19104, USA
** *Present address:* Groupe de Physique Appliquée, Université de Genève, CH-1211 Genève 4, Switzerland

[14–17]. Similarly, pulse delay and pulse stretching were carefully measured in well-characterized aqueous suspensions of particles by various groups [18–20]. The reduction due to multiple scattering of the apparent particulate extinction derived from transmittance and target-reflectance measurements was investigated in laboratory experiments by Ivanov and Khairullina [21], Khairullina and Ivanov [22], Battistelli et al. [23], and Smith and Carswell [24]. Finally, the multiple forward-scattering effect on image transmission was studied in detail by the Modulation Transfer Function (MTF) measurements through aqueous suspensions of polystyrene microspheres [25].

All these measurements clearly demonstrate the diversity and importance of the multiple-scattering effects and the necessity of adequate modeling, either to predict the various contributions described above or to make use of them to derive information on the aerosol parameters. A great deal of progress has been made over the past 15–20 years. In this respect, it is important to recall the early work performed in the Former Soviet Union on Monte-Carlo and asymptotic methods, as described, for example, in [26–28]. However, a complete review of all theoretical models is beyond the scope of this article. Instead, we want to report on a concerted research effort initiated under a bilateral German-Israeli cooperation that has since evolved into an informal but more international group. The group holds the annual MUSCLE workshops. Its aim is to stimulate experimental as well as theoretical work to better understand and make use of the measured multiple-scattering LIDAR contributions for maximizing our information on lidar probing of cloud and fog microphysical parameters.

Various theoretical approaches are currently being pursued within the MUSCLE group. One common feature is that they all need some form of approximation or specialization to make the solution computionally possible or affordable. Validation is therefore necessary. Most models have already been compared to experimental data or other theoretical calculations but, since these comparisons generally address different aspects of multiple scattering, it is difficult to appreciate the relative performance of the models. Confronted with this difficulty, the group has decided to apply all models and algorithms to a common problem. The area of interest is LIDAR backscatter and, in the absence of a sufficiently complete set of experimental multiple-scattering LIDAR data at the time of definition of the task, a numerical experiment was chosen as a valid and convenient alternative. All participants were to calculate the LIDAR returns for the same specified cloud, instrument and geometrical parameters. The purpose of this and the other articles in this Feature Issue of *Applied Physics B* is to report on the results of the exercise. The direct problem was chosen because few multiple-scattering inversion methods exist yet; in fact, they depend on the successful test of the direct methods.

The common problem is defined in Sect. 1. Section 2 gives a brief outline of the individual theoretical models, which are described at length in the remaining articles of this issue. The comparison results are presented and discussed in Sect. 3.

## 1 Numerical experiment

The numerical experiment consists in calculating the LIDAR returns from a 300 m thick, uniform density, Deirmendjian [29] C.1 cloud defined by the droplet-size distribution

$$\frac{dn}{dr} = Cr^6 \exp(-1.5r), \tag{1}$$

where $r$ is the droplet radius and $C$ is a constant. The cloud is at a height $H$ of 1000 m from the LIDAR transceiver and the atmosphere below does neither absorb nor scatter.

The LIDAR transmitter is a pulsed Nd:YAG 1.064 $\mu$m laser. The beam has a Gaussian profile of vanishing beam waist and a divergence equal to 0.1 mrad full angle. It is directed perpendicularly to the base of the cloud. The pulse length $\mathscr{T}$ is 40 ns for a spatial resolution $c\mathscr{T}/2$ of 6 m, where $c$ is the speed of light.

The receiver is coaxial with the laser. The LIDAR returns are to be calculated per unit aperture area for a vanishingly small aperture size. Two fields of view are specified: 1 and 10 mrad full angle.

The cloud's scattering properties were calculated with Mie theory. The particle refractive index was taken as $m = 1.325 + 0\mathrm{i}$ and the constant $C$ of (1) was adjusted to give an extinction coefficient of 17.25 $\mathrm{km}^{-1}$. The size distribution was cut off at 0.001 $\mu$m at the low end and 20 $\mu$m at the high end. The angular phase function was calculated with a resolution of 1° and distributed to all participants. To minimize discretization errors and to satisfy their model needs, the Florence group recalculated the full scattering matrix at 1000-point resolution. The other groups used interpolation except for the Swiss group whose model calculates the scattering contributions from the analytic size distribution directly, i.e., (1). Summation or integration was performed to compute the LIDAR return over the 40 ns length of the laser pulse.

The calculated multiple-scattering (all considered orders) LIDAR returns per unit receiver aperture area is normalized by the single scattering return $\mathscr{L}_{ss}$ per unit area given by

$$\frac{\mathscr{L}_{ss}(z)}{A} = \frac{1}{(H+z)^2}\frac{c\mathscr{T}}{2}\sigma_s P(\pi)\exp(-2\sigma_e z), \tag{2}$$

where $A$ is the aperture area, $z$ is the range inside the cloud, $H = 1000$ m is the distance to the base of the cloud, $c\mathscr{T}/2 = 6$ m is the spatial resolution of the lidar, $\sigma_s$ is the cloud-scattering coefficient equal here to the extinction coefficient $\sigma_e = 17.25\ \mathrm{km}^{-1}$, and $P(\pi) = 0.0555058$ is the scattering phase function at 180°. The phase function is normalized such that

$$\frac{1}{2}\int_0^\pi P(\theta)\sin\theta\, d\theta = 1. \tag{3}$$

Model permitting, the lidar returns for the first two orders of scattering are also computed for evaluation of the relative importance of the higher scattering orders.

## 2 Models

The models used in this numerical experiment fall under four main categories: numerical Monte-Carlo calculations, stochastic description of photon scattering, analytical extension of the Mie theory, and approximations to the radiative-transfer equation.

### *2.1 Florence group's Monte-Carlo model*

The model used by the Florence group [30] is a semi-analytic Monte-Carlo method in which the contributions of the different orders of scattering to the LIDAR returns are calculated separately. The polarization of the returned radiation is taken into account by using the Stokes vectors and scattering matrices to represent the probability of photon scatterings in the different spatial directions.

The variance of the results is reduced by one of the following techniques. In the first technique, relations are established to scale the calculations of LIDAR returns made at different extinction coefficients for different scattering orders to a common extinction value. The second technique is based on the use of a distorted phase function according to a method first proposed by Platt [31]. The distorted phase function, which is made symmetrical about the scattering angle of 90°, increases the probability of photons scattered in the backward direction near the reversed axis of the laser beam. For the results presented here and in their paper [30], the Florence group used the second variance-reduction procedure. Regarding polarization, some second-order Monte-Carlo calculations were also compared with an analytic integration formula [32].

Although this is not of direct interest to the present comparison of homogeneous cloud calculation results, some simple cases of inhomogeneous cloud geometry can be dealt with by the Florence group Monte-Carlo code.

### *2.2 NASA Langley group's Monte-Carlo model*

The approach used by the NASA group [33] is a Monte-Carlo simulation of the physical scattering process [34]. Unlike the Florence group, no variance-reduction techniques are used. While inefficient for problems where the dimensions of the scattering volume are less than the length of the photon mean free path, the procedure is straightforward and can be used as a check against more sophisticated approaches which may be subject to statistical bias. The only inputs required are the volume extinction cross section and single-scatter albedo of the medium, and the single-scatter phase function. Photon trajectories are constructed and the path of each transmitted photon is followed from the transmitter through multiple scatterings in the cloud. To improve computational efficiency to the point where the calculation is practical, each time a photon scatters, the probability of the photon scattering directly back to the receiver is computed analytically. This probability value is added to the detector signal and the statistical weight of the photon is reduced. The sum over all scattering events for all photons represents the LIDAR signal. The first thirty orders of scattering were included in the calculations presented below. Two million photon trajectories were constructed for each case, producing returns to a depth of several hundred meters with acceptably low noise. It was found that the first 4 orders of scattering were sufficient to describe the 1 mrad case and 10 orders were required for the 10 mrad case.

### *2.3 Munich group's stochastic model*

The model of the Munich group [35] starts from a description of the process of multiple scattering by a stochastic model from which a general formula for the multiply scattered LIDAR return signal is derived. In principle, the terms describing the contributions of the different scattering orders of this formula may be calculated by analytical methods (for lower scattering orders only), or by Monte-Carlo simulation of the physical process.

The main drawback of the "physical" Monte-Carlo method is often too expensive cost for calculations with desired accuracy. This is not connected with the slow convergence of the method, but because a great part of computational capacity is wasted for the simulation of unimportant or statistically insignificant events. The means to make the Monte-Carlo method interesting for calculations is to concentrate on the significant aspects of the problem. Such a technique reduces the statistical variance for the same amount of computer time, i.e., it increases the efficiency of the computational scheme.

For reducing the variance-weigth Monte-Carlo algorithms are used with "non-physical" probability distributions. These distributions are constructed properly from the a-priori information of the photons' importance. Simultaneously, weigth multipliers are introduced correcting the bias of the estimators. Each photon history is marked with its weight, which, in some sense, represents the number of simulated photons. The variance-reduction computational schemes are based on the simulation of the transport of a large number of photons with relatively low weights in interesting regions, and the introduction of only a small number of photons with relatively high weights in unimportant regions.

### *2.4 Israel group's Monte-Carlo model*

The geometry for the Israel group's Monte-Carlo method is discussed in [36]. The sum of all possible multiple-scattering events resulting in a simultaneous signal at the receiver is evaluated by using the Monte-Carlo statistical technique. The number $N$ of randomly chosen scattering positions inside the clouds are selected by the computer. All multiple-scattering contributions for which the sum of all distances from the source through the $N$ scatterers to the receiver is constant within the time and spatial resolutions of the system are then added for simultaneous collection.

### 2.5 Swiss group's analytical extension of Mie theory

The approach adopted by the Swiss group [38] is based on an analytical extension of Mie theory to include the effects of multiple scattering. As it is well known, Mie theory describes the field arising from the scattering of a plane wave incident upon a sphere [37]. Depending on the density of the medium, the scattered field can be rescattered by other particles. We have then double scattering. In the approach described in [38], the spherical wave scattered by the first particle is considered as the field impinging on the second one. This procedure can be repeated at all scattering orders. Notice that in the case of higher scattering orders, the incident field is a superposition of spherical waves. Following analytically this process step by step we construct the $n$-fold electromagnetic field scattered by an ensemble of particles. The physical quantities of interest are expressed by a straightforward generalization of the corresponding single-scattering quantities and the multiple-scattering process is described without losing the advantage of working with analytical expressions in the frame of Mie theory. This approach differs from both the numerical and analytical models presented in this paper in several respects. The multiple-scattering contributions to the intensity are calculated from a general expression of the $n$-fold scattered field, which is derived without using far-field or small-angle approximations [39]. In particular, it allows to calculate the multiple-scattering contributions due to each single particle as well as the total contributions of the whole medium. There are also a few similarities, as discussed in [39]. A comparison with the statistical approaches shows some common features, namely the primary interaction derived from single-scattering results and the process of averaging based on the distribution of scatterers. However, it is dealing with analytical expressions at each stage of the procedure and the average quantities are calculated only at the end. This leads to a great simplification of the numerical procedures. In addition, the model uses radiative-transfer theory to derive the multiple-scattering LIDAR equation [39]. The beam intensity $I(z, t)$ impinging on a slab of thickness $dz$ results from the total aerosol attenuation including the multiple forward-scattering contributions to the extinction coefficient, while only single-scattering extinction is usually considered. The multiple-scattering LIDAR equation follows from this generalized transfer equation by formal integration [39]. The required inputs are the LIDAR-system parameters, and the aerosol particle-size distribution and number density. In atmospheric problems, the method applies uniformly and does not suffer from the convergence and stability problems caused by the large number of events that normally have to be taken into account at large optical depths and in the presence of strong experimental noise. Moreover, the absence of small-angle approximations allows accurate evaluation of the multiple-scattering contributions, for instance in space-borne applications.

### 2.6 DREV group's radiative-transfer model

The DREV (Defence Research Establishment Valcartier) model [40] is an approximation to the radiative-transfer equation applicable to narrow incident light beams. The method relies on two main hypotheses. The paraxial approximation and the representation of the flux normal to the incident beam axis by a diffusion process. The model solutions are the forward- and backscattered intensity profiles. The required inputs are the LIDAR-system parameters, and the aerosol single-scattering angular phase function and extinction and scattering coefficients, which are allowed to vary along the beam axis. On the basis of comparisons with forward- and backscattering measurements made in the laboratory and the atmosphere [40], the solutions are valid for optical depths smaller than $\approx 10$, for phase functions corresponding to average size parameters of order one or greater, and for off-axis positions not exceeding $\approx 25\%$ of the reciprocal of the scattering coefficient.

### 2.7 Minsk group's radiative-transfer model

The semianalytic radiative-transfer approach developed by Zege et al. [41] is based on the following model. The radiance in the forward direction is due to small-angle multiple scattering, whereas only single scattering is taken into account in the backward hemisphere. With the use of the reciprocity theorem and the aspect-invariance property [28] of systems, the following simple expression for the LIDAR return was obtained

$$F(t=2z/c) = \sigma_s \int d\mathbf{n}\, P_\pi(\mathbf{n}) I(2z, \mathbf{r}=0, \mathbf{n}), \tag{4}$$

where $\sigma_s$ is the cloud scattering coefficient, $P_\pi(\mathbf{n})$ is the phase function in the backward hemisphere, $I(2z, \mathbf{r}=0, \mathbf{n})$ is the on-axis ($\mathbf{r}=0$) angular radiance distribution at range $2z$ inside the cloud due to some effective source. This effective source has the spatial-angular radiance profile

$$W(\mathbf{r}, \mathbf{n}) = \int d\mathbf{r}' \int d\mathbf{n}'\, W_r(\mathbf{r}', \mathbf{n}')\, W_s(\mathbf{r}-\mathbf{r}', \mathbf{n}-\mathbf{n}'), \tag{5}$$

where $W_s(\mathbf{r}, \mathbf{n})$ and $W_r(\mathbf{r}, \mathbf{n})$ are the profiles of the source and the receiver, respectively. For a monostatic LIDAR, the center and the axis of this effective source coincide with those of the laser.

Theoretical estimations and comparisons with available data show that this model should give high accuracy up to $t \approx 15/\sigma_s c$ at $g > 0.8$, where

$$g = \frac{1}{2} \int d\theta \sin(\theta) \cos(\theta) P(\theta)$$

is the asymmetry parameter of the phase function.

Two approaches to estimate the value of $I(2z, \mathbf{r}=0, \mathbf{n})$ in (4) have been developed. Both of them rely upon the multicomponent method of the radiative-transfer equation solution [42]. In the fully analytic solution [41], the small-angle diffusion approximation was used to estimate the components. Here, more accurate

data are presented, where the integrand $I(2z, \mathbf{r} = 0, \mathbf{n})$ was calculated through the multicomponent small-angle solution, and the problem of evaluating a three-dimensional integral arose [41]. The required inputs are the LIDAR-system parameters, the aerosol phase function and extinction and scattering coefficients which are allowed to vary along the beam axis.

## 3 Comparison results

The comparison results are plotted in Figs. 1–4 for the 10 and 1 mrad field-of-view multiple-to-single and double-to-single scattering LIDAR return ratios, respectively. These curves are a measure of the relative importance of multiple-scattering contributions in LIDAR signals. They give, for each range $z$ into the cloud, the multiple- or double-scattering content of the LIDAR return in terms of the corresponding single-scattering value calculated from (2). All curves have the same characteristic shape, i.e., a rapid rise for the first few tens of meters (optical depth $<0.5$) followed by a more gentle and progressively smaller and smaller rate of increase. In the simulation example of this paper, the ratio reaches values of $\approx 10$ in the 10 mrad case and slightly below 1 in the 1 mrad case. A first conclusion, therefore, is that higher-order scattering is significant and a strong function of the receiver field of view. Clearly, for the cloud property and LIDAR geometry chosen here, it could not be neglected in the process of inverting the LIDAR return for retrieving the cloud extinction coefficient.

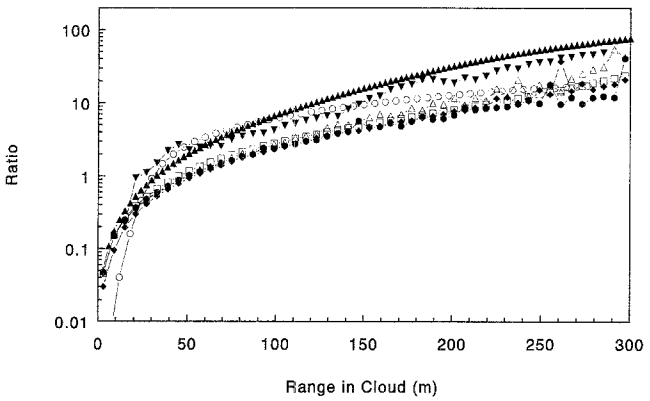


**Fig. 1.** Calculated ratios of the multiple-to-single scattering contributions to the LIDAR return from a uniform C.1 cloud for a receiver field of view of 10 mrad; the cloud base is at 1 km and the LIDAR is directed vertically. (▲, DREV's model; ●, Florence group's model; ▼, Israel group's model; ◆, Munich group's model; △, NASA group's model; ○, Swiss group's model; □, Minsk group's model)

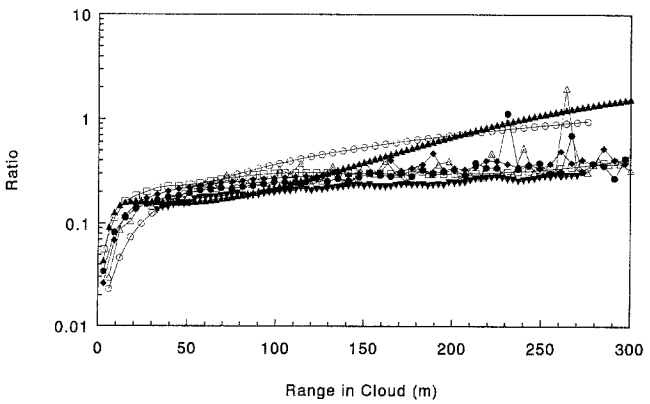


**Fig. 2.** Same as Fig. 1 but for a receiver field of view of 1 mrad

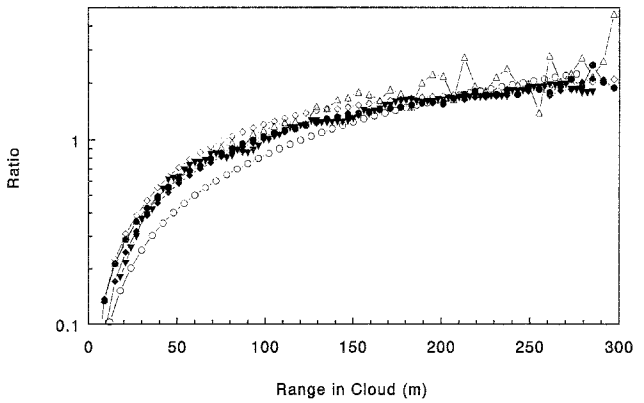


**Fig. 3.** Calculated ratios of the double-to-single scattering contributions to the LIDAR return from a uniform C.1 cloud for a receiver field of view of 10 mrad; the cloud base is at 1 km and the LIDAR is directed vertically. (Symbols as in Fig. 1)

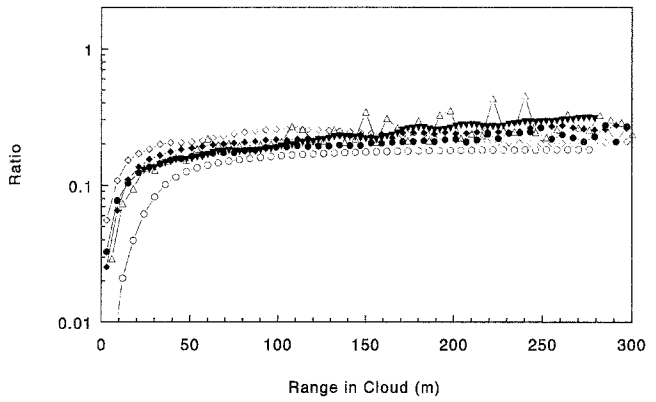


**Fig. 4.** Same as Fig. 3 but for a receiver field of view of 1 mrad

There is close agreement between the results of the Florence, Munich, NASA and Minsk groups for all cases. The first three groups use similar Monte-Carlo methods that, however, differ in their calculation algorithms. The Minsk group's is a semianalytic approximation to the radiative-transfer equation. This good agreement between different approaches is certainly a worthwhile achievement. In the other cases, the level of agreement varies from one situation to the other. For example, the Israel group's Monte-Carlo calculations agree with Florence's, Munich's and NASA's for double scattering and for multiple scattering at 1 mrad but are higher for multiple scattering at 10 mrad. The DREV's radiative-transfer model gives multiple-scattering contributions that are generally on the high side as compared with the other results; at 10 mrad, there is reasonable

agreement with the Israel group's calculations, whereas at 1 mrad, the shape of the curve is slightly different than for the other models showing a greater asymptotic rate of increase. The results of the Swiss group show generally a lower rise in the first part of the curves and converge to the results of the other groups after a few tens of meters. For double scattering and multiple scattering at 10 mrad, the results are very similar to the other models and the curves merge after the first meters. For multiple scattering at 1 mrad, the results are slightly higher for the range from 100 to 200 m, and similar to the DREV results from 200 to 300 m. We have no independent information to determine which, if any, of these models gives the right answer, but the results are a good indication of the difficulties of predicting higher-order scattering in all its aspects. Figures 1–4 show 4 different but still related situations and yet we find that the disrepancies do not obey a fixed pattern; models that agree in one situation may disagree in the other.

Following are a few thoughts on the origin of the differences. To generalize somewhat the discussions, the results are regrouped under three categories.

### *3.1 Monte-Carlo results*

The first group of models has in common the application of Monte-Carlo techniques in one form or the other. A main advantage of these techniques is that they allow the calculation of the solutions with the desired accuracy. The Monte-Carlo approach is based on computer simulation of photon trajectories. The expected values of the signals are estimated by averaging over the ensemble of independent samples. In analog simulation, the elements of the trajectories, i.e., the free-path length and the scattering angle, are chosen from the probability distributions of the corresponding physical parameters. The constructed random trajectories are statistically equivalent to those of the real photons. The analog method is relatively simple to implement but its main drawback is the calculation time to achieve the desired accuracy. In the LIDAR geometry of interest here, this is due to the high anisotropy of light scattering in clouds. The probability of backscattering is extremely small so that the detections of physical photons are statistically rare events. As a consequence, the variance of the calculated signals is high and it improves only as $1/\sqrt{N}$, where $N$ is the number of samples. To reduce the variance, weighted Monte-Carlo methods are used. They are based on employing "non-physical" probability distributions. Simultaneously, corresponding weight multipliers are introduced to correct for the bias of the estimators. The result is a reduction of the statistical variance for the same amount of computation time. This means increasing the efficiency of the computational algorithms.

In view of the differences shown in Figs. 1–4, it is important to recall briefly the variance-reduction methods used in the Monte-Carlo calculations of this paper. The following methods were applied at various stages of the calculations:

*3.1.1 Semianalytical method [30, 33].* This method consists in calculating analytically, from the scattering distribution at each scattering point, the probability of hitting the receiver with no further scattering events. For the practical application of this paper (small-aperture receiver located far from the scattering points), this method reduces the variance compared with the analog Monte-Carlo method, because in the latter case the events of photons hitting the receiver aperture are very rare.

*3.1.2 Point-flux estimator [35].* This method is based on the exact calculation of the flux density at a given point in space. For a ring receiver, the calculations are carried out by randomly choosing a point on the ring.

Although the above methods reduce the variance, they are often not sufficient. To speed up the computations even more, additional variance-reduction techniques have been implemented.

*3.1.3 Angular bias [30].* This method has been directly derived from that introduced by Platt [31] and consists in using a fictitious phase function distorted in order to increase the probability of photons undergoing scattering with angles in the backward direction. As in [31], a phase function is employed which is obtained by leaving the original phase function unchanged between $\theta = 0$ and $\pi/2$, where $\theta$ is the scattering angle, and letting $P(\theta)$ be equal to $P(\pi - \theta)$ in the backward hemisphere. The resulting function is then renormalized. It is, however, necessary to apply suitable weights to the photons at each scattering angle. Thus, for each trajectory, the photon carries the product of the weights pertaining to the preceding scattering events and changing along its trajectory.

*3.1.4 Scaling relationship [30].* In this method, the contributions to the LIDAR returns for each scattering order are calculated at a different value of the optical depth $\tau$ of the considered cloud layer. Generally, $\tau$ is taken nearly equal to the scattering order. Then, the returns are scaled to the desired common value of $\tau$, as explained in [30]. This procedure proved useful in reducing the number of photon trajectories necessary to achieve the desired convergence of the calculations. Tests on the angular bias and scaling procedures showed that their relative efficiency depends, among other factors, very much on the order of scattering. Generally, for contributions of scattering orders greater than about 6, the scaling relations are more effective than the angular-bias procedure.

*3.1.5 Splitting of scattering [35].* Another variance-reduction tool is based on angle splitting at the points of scattering near the laser axis. The incident trajectory is split into two trajectories: a first one into the cone near the backward direction and a second one in the remaining portion of the sphere. The angles of the split trajectories are picked out according to the angular distributions proportional to the phase functions $P(\pi - \theta)$ and $P(\theta)$, respectively. The weight factors of both trajectories are less than unity. Splitting of scattering essentially increases the number of photons backscattered into the detector directions. The speed-up in the computations for the case of the 10 mrad receiver field of view is in the

range of 8–25 times faster than for the corresponding analog code.

*3.1.6 Exponential transformation with point splitting and Russian roulette [35].* The exponential transformation is a photon free-path length stretching method. The sampled path length in the random walk is stretched in the preferred direction to the receiver and reduced in the opposite direction. The weight at the end of the path is the product of an exponential function and an angular factor. The exponential function is the ratio of the values of the exponential transformant at the beginning and end points of the path. The angular factor $v$ follows the general rule that it is larger than unity if the angle $\Omega$ between the direction of the photon path and the line to the detector is less than $\pi/2$, and smaller than unity if $\Omega > \pi/2$. In their code, the Munich group used the combination of the exponential transformation with splitting and Russian roulette. If a photon moves toward the receiver, i.e., $\Omega < \pi/2$, they simulate the splitting into $v$ photons, and if it moves away from the detector, i.e., $\Omega > \pi/2$, they simulate the Russian roulette with survival probability $v$. The speed-up of the computations by this method combined with splitting of scattering is of the order of 2–5 times faster than the corresponding calculations with splitting alone.

The accompanying papers of this issue describe in more detail how these variance-reduction algorithms were implemented. Here, we want to emphasize that they are specialized representations of the scattering interactions that involve some degree of approximation. Since the actual algorithms are different from model to model, they could explain some of the differences observed in the solutions plotted in Figs. 1–4. Other causes are the differences in the basic models themselves. For example, the Israel approach is not the classical photon-trajectory simulation described above, but a volume random selection of scattering centers in number equal to the scattering order and sorted to give the same total propagation length. Finally, there could also be errors due to the angular resolution used for the numerical evaluation of the phase function near the forward peak. Unfortunately, the same resolution was not used everywhere. For all these reasons, the differences observed among the Monte-Carlo results of Figs. 1–4 are not unreasonable.

### *3.2 Recursive Mie results*

The main feature of our approach is the analytical generalization of the scattered electromagnetic field to include the contributions of multiple-scattering processes. The basic expressions are derived in a very general context without using far-field or small-angle approximations. Moreover, the general expression of the field leads to account for interference effects between the contributions from the fields at different scattering orders. In the particular case of the LIDAR experiment considered here, the total scattered intensity has been calculated from the expression of the amplitude of the total scattered field using some approximations compatible with the particular experiment and the major assumptions used by other groups [39]. The results, which are in good agreement with the other proposed methods, are valid in the framework of these approximations. However, they leave the way open to more general and accurate calculations. The discrepancies at "short" distances are related to the different dependence on the receiver field of view in the Swiss model, which results from the approximations made in the numerical calculations, as discussed in [39].

### *3.3 Radiative-transfer results*

Although derived from the same radiative-transfer equation, the DREV's and Minsk's algorithms are rather different, as the individual papers [40, 41] show. The differences in the results are therefore not surprising. The solutions have the same general shape but they turn out to be approximately the lower and upper limits of all models considered here. The principal characteristic of the DREV's model is the ad hoc or phenomenological representation of beam spreading by a lateral diffusion process based on the analogy with the successful modeling of transport processes in turbulence. The model calculates all multiple scatterings at once and cannot single out the contributions from the various orders. In the Minsk's approach, the spatial angular spread is separated into two regimes: in the very near forward direction, the small-angle approximation is assumed, whereas, at larger angles, only single scatterings are taken into account. For this reason, the model underestimates the multiple-scattering contributions at large time and wide fields of view but should give accurate results within the limits discussed in [41]. Computationally, the phase function is separated into linear components that satisfy the two-regime description of angular scattering but that also provide an efficient algorithm for handling the multidimensional integral in the radiative-transfer equation. Therefore, the radiative-transfer equation is solved by two very different algorithms and the levels of accuracy achieved by the lateral diffusion model in the first case and the multicomponent representation of the phase function in the second are certainly not uniform for all aspects of multiple scattering, and the two approaches can give different answers in any given application, as shown here.

The Minsk's results are very close to the Monte-Carlo calculations of the Florence, Munich and NASA groups. The four together represent the lower limit of the calculated multiple-to-single scattering ratios of this paper.

The DREV's model was validated by comparison with experimental data [40] for many different forward- and backscattering problems. The agreement is quite consistent over all situations considered but it is no better than a factor of $\approx 1.5$, which is actually of the same order as the scatter of the experimental data. In one example, the DREV's solutions were coompared with laboratory LIDAR-simulation data in a geometry that emulates that of our numerical example of Fig. 1. In conditions of large multiple-scattering contributions, the solutions turned out to be larger than the measurements by a factor of $\approx 1.5$ or less, as illustrated in Fig. 7 of [40]. If extrapolated to the problem of Fig. 1, these experimental data would fall approximately half way between the

DREV's and Minsk's solutions which, as mentioned earlier, represent approximately the upper and lower limits of all plotted solutions. We can, therefore, conclude that the differences between the radiative-transfer models of Figs. 1 and 2 are not large compared with the observed experimental uncertainties of the measurements reported in [40], and that the applicable measurements happen to fall well within the scatter among all models. A main advantage of the radiative-transfer algorithms is that they required insignificant computation time.

## 4 Conclusions

The calculations of this paper are a very worthwhile exercise for LIDAR users. The LIDAR community needs improved and validated models of LIDAR measurements in varied aerosol conditions, especially as regards the importance of multiple scattering. While limited in scope, the project described here was a first attempt at pulling together a wide-enough spectrum of modeling approaches to address multiple-scattering effects on LIDAR operation. The exercise has contributed a concensus of results and understandings which should help take the multiple-scattering contributions into account in LIDAR applications, and eventually make use of the information they contain. Clearly, and independently of the level of agreement, the calculations of Figs. 1–4 show that higher-order scattering can contribute to measured LIDAR returns to a level that cannot be neglected in inversion algorithms. The problem chosen here is only one among a whole set of practical scenarios and probably a favorable one in terms of the magnitude of the multiple-scattering effects. For example, a space-based application with greater LIDAR-to-cloud distance would lead to much larger multiple-scattering effects for otherwise identical parameters. The comparisons show excellent agreement between some of the models in some cases, but disagreement, sometimes between the same models, in other cases. Obviously, the calculation differences stem from differences in the models and/or algorithms, as explained in the preceding section. Higher-order scattering depends on a large number of local and path-integrated aerosol properties as well as on the geometry of the problem. Consequently, models and algorithms require simplifications or expedients and it seems, from the results of our intercomparison, that it is very difficult to reproduce all aspects with uniform accuracy. The intercomparison has allowed us to take a closer look at the model particularities that could explain the observed differences. The difficulty in implementing corrections is to determine which is the true solution. More measurements in well-controlled and varied conditions are now necessary. It is hoped that the present results will stir further interest in improving and validating our and other multiple-scattering models and calculation algorithms. This is essential for the accurate determination of aerosol properties from LIDAR measurements in moderate to dense concentrations, in particular for cloud studies.

## References


1. V.A. Donchenko, I.V. Samokhvalov, G.S. Matvienko: Izv. Akad. Nauk SSSR, Fiz. Atmos. Okeana **7**, 1183 (1971)
2. G.M. Kaul, I.V. Samokhvalov: Izv. Vuzov, Ser. Fiz. **8**, 109 (1975)
3. E.A. Bucher, R.M. Lerner: Appl. Opt. **12**, 2401 (1973)
4. G.C. Mooradian, M. Geller, L.B. Stotts, D.H. Stephens, R.A. Krautwald: Appl. Opt. **18**, 429 (1979)
5. R.J. Allen, C.M.R. Platt: Appl. Opt. **16**, 3193 (1977)
6. S.R. Pal, A.I. Carswell: Appl. Opt. **17**, 2321 (1978)
7. L.R. Bissonnette, D.L. Hutt: Appl. Opt. **29**, 5045 (1990)
8. C. Werner, J. Streicher, H. Herrmann, H.-G. Dahn: Opt. Eng. **31**, 1731 (1992)
9. N.S. Kopeika, S. Solomon, Y. Gencay: J. Opt. Soc. Am. **71**, 892 (1981)
10. L.R. Bissonnette: Opt. Eng. **31**, 1045 (1992)
11. L.W. Winchester, G.G. Gimmestad: Opt. Eng. **22**, 86 (1983)
12. M.A. Seagraves, J.F. Ebersole: Opt. Eng. **22**, 90 (1983)
13. D.L. Hutt, L.R. Bissonnette, D. St.-Germain, J. Oman: Appl. Opt. **31**, 5121 (1992)
14. J.S. Ryan, A.I. Carswell: J. Opt. Soc. Am. **68**, 900 (1978)
15. J.S. Ryan, A.I. Carswell: J. Opt. Soc. Am. **69**, 60 (1979)
16. R.B. Smith, A.I. Carswell: Appl. Opt. **24**, 3546 (1985)
17. L.R. Bissonnette, R.B. Smith, A. Ulitsky, J.D. Houston, A.I. Carswell: Appl. Opt. **27**, 2485 (1988)
18. Y. Kuga, A. Ishimaru: J. Opt. Soc. Am. **73**, 1812 (1983)
19. R.A. Elliott: Appl. Opt. **22**, 2670 (1983)
20. G. Zaccanti, P. Bruscaglioni, M. Dami: Appl. Opt. **29**, 3938 (1990)
21. A.P. Ivanov, A.Ja. Khairullina: Izv. Akad. Nauk SSSR Fiz. Atmos Okeana **2**, 721 (1966)
22. A.Ja. Khairullina, A.P. Ivanov: Zh. Prikl. Spektrosk. **7**, 255 (1967)
23. E. Battistelli, P. Bruscaglioni, A. Ismaelli, L. LoPorto, G. Zaccanti: Appl. Opt. **25**, 420 (1986)
24. R.B. Smith, A.I. Carswell: Appl. Opt. **25**, 398 (1986)
25. Y. Kuga, A. Ishimaru: J. Opt. Soc. Am. A **2**, 2330 (1985)
26. E.P. Zege, A.P. Ivanov, I.L. Katsev, B.A. Kargin, G.A. Mikhailov: Izv. Akad. Nauk SSSR Fiz. Atmos. Okeana **9**, 1054 (1973)
27. G.I. Marchuk, G.A. Mikhailov, M.A. Nazarliev, R.A. Darbinyan, B.A. Kargin, B.S. Elepov: *The Monte-Carlo Methods in Atmospheric Optics,* Springer Ser. Opt. Sci., Vol. 12 (Springer, Berlin, Heidelberg 1980)
28. E.P. Zege, A.P. Ivanov, I.L. Katsev: *Image Transfer Through a Scattering Medium* (Springer, Berlin, Heidelberg 1991)
29. D. Deirmendjian: J. Appl. Meteorol. **14**, 1584 (1975)
30. P. Bruscaglioni, A. Ismaelli, G. Zaccanti: Appl. Phys. B **60**, 325 (1995)
31. C.M.R. Platt: J. Atmos. Sci. **38**, 156 (1981)
32. P. Bruscaglioni: Opt. Commun. **27**, 9 (1978)
    G. Zaccanti: Depolarization and Double Scattering from Fog, Report IV/A/2.9 (Univ. Florence, Florence 1979) (in Italian)
33. D. Winker, L.R. Poole: Appl. Phys. B **60**, 341 (1995)
34. L.R. Poole, D.D. Venable, J.W. Campbell: Appl. Opt. **20**, 3653 (1981)
35. U.G. Oppel, A.V. Starkov, M. Noormohammadian: Appl. Phys. B **60**, 335 (1995)
36. A. Cohen, M. Kleiman, J. Cooney: Appl. Opt. **16**, 1905 (1978)
37. G. Mie: Ann. Phys. **25**, 377 (1908)
38. C. Flesia, P. Schwendimann: Appl. Phys. B **56**, 157 (1993)
39. C. Flesia, P. Schwendimann: Appl. Phys. B **60**, 331 (1995)
40. L.R. Bissonnette: Appl. Phys. B **60**, 315 (1995)
41. E.P. Zege, I.L. Katsev, I.N. Polonsky: Appl. Phys. B **60**, 345 (1995)
42. E.P. Zege, I.L. Katsev, I.N. Polonsky: Appl. Opt. **32**, 2803 (1993)